

The Conversion of CO₂ to Methanol on orthorhombic β-Mo₂C and Cu/β-Mo₂C Catalysts: Mechanism for Admetal Induced Change in the Selectivity and Activity

Sergio Posada-Pérez,^a Pedro J. Ramírez,^b Ramón A. Gutiérrez,^b Dario J. Stacchiola,^c Francesc Viñes,^{a,*} Ping Liu,^c Francesc Illas^a and José A. Rodríguez^{c,*}

^a *Departament de Química Física & Institut de Química Teòrica i Computacional (IQTCUB), Universitat de Barcelona, c/ Martí i Franquès 1, 08028 Barcelona, Spain*

^b *Facultad de Ciencias, Universidad Central de Venezuela, Caracas 1020-A, Venezuela*

^c *Chemistry Department, Brookhaven National Laboratory, Upton, NY 11973, USA*

Abstract

The conversion of CO₂ into methanol catalyzed by β-Mo₂C and Cu/β-Mo₂C surfaces has been investigated by means of a combined experimental and theoretical study. Experiments have shown the direct activation and dissociation of the CO₂ molecule on bare β-Mo₂C, whereas on Cu/β-Mo₂C, CO₂ must be assisted by hydrogen for its conversion. Methane and CO are the main products on the clean surface and methanol production is lower. However, the deposition of Cu clusters avoids methane formation and increases methanol production even above that corresponding to a model of the technical catalyst. DFT calculations on surface models of both possible C- and Mo-terminations, corroborate the experimental observations. Calculations for the clean Mo-terminated surface reveal the existence of two possible routes for methane production ($C + 4H \rightarrow CH_4$; $CH_3O + 3H \rightarrow CH_4 + H_2O$) which are competitive with methanol synthesis, displaying slightly lower energy barriers. On the other hand, a model for Cu deposited clusters on the Mo-terminated surface points towards a new route for methanol and CO production avoiding methane formation. The new route is a direct consequence of the generation of a Mo₂C-Cu interface. The present experimental and theoretical results entail the interesting catalytic properties of Mo₂C as an active support of metallic nanoparticles, and also illustrate how the deposition of a metal can drastically change the activity and selectivity of a carbide substrate for CO₂ hydrogenation.

* **Corresponding authors:** francesc.vines@ub.edu; rodrigez@bnl.gov

Keywords: CO₂ activation, CO₂ hydrogenation; methanol; methane; reverse water-gas shift reaction; metal carbides; copper

I. Introduction

Carbon dioxide (CO_2) is one of the major pollutants in the atmosphere produced as a consequence of the combustion of fossil fuels in industrial processes, vehicles and household operations.^{1,2} Over the years, it has become clear that transition metal carbides (TMC) can be quite useful for the transformation of CO_2 into CO, methanol, methane and other hydrocarbons.³⁻⁹ They can be used as supports for the dispersion of metals or as catalysts on their own.^{3,5-7,10} As substrates, TMC can enhance the reactivity of a supported metal through strong metal-support interactions.^{3,11}

The metal/carbon ratio in a carbide can have a strong effect in the reactivity of the system towards CO_2 .^{12,13} Carbides with metal/carbon ratio of one usually adsorb CO_2 without cleaving the C-O bonds in the molecule.^{12,14} For example, on the TiC(001) and δ -MoC(001) surfaces, theoretical calculations show an activation of the molecule but the C-O bonds do not break.^{12,14} The interaction of the C atom in CO_2 and a C atom in the carbide surface leads to the formation of a regular C-C bond; there is a net charge transfer from the surface to CO_2 and the O-C-O bond angle decreases from 180° in gas phase to $\sim 125^\circ$ in the TMC surface. Consequently, the adsorbed molecule can be described as a carboxylate ($\text{CO}_2^{\delta-}$) species.^{12,14} The dissociation of this species is not spontaneous but C-O bond cleavage can be induced through reaction with hydrogen and formation of a COOH intermediate.¹⁵ A higher reactivity towards CO_2 has been observed in TMC with a metal/carbon ratio close to 2.^{6,12,13} In the case of the β - Mo_2C (001) system, the surface can have metal and carbon terminations.^{12,16,17} In a β - Mo_2C (001)-Mo surface, the exposed Mo atoms partially dissociate CO_2 at low temperature (< 300 K) and the CO produced also can decompose into C and O adatoms by overcoming a relatively small (~ 1 eV) energy

barrier.^{12,18} Thus, the hydrogenation of CO₂ on a Mo-terminated β -Mo₂C(001) can produce CO, CH₄ and CH₃OH as reaction products. On the other hand, the C-terminated β -Mo₂C(001) surface is not so reactive towards CO₂ decomposition and the CO/CH₄/CH₃OH ratio in the CO₂ hydrogenation products is expected to be significantly different from that corresponding to the β -Mo₂C(001)-Mo surface.¹²

In practical terms, it is sometimes desirable to couple the high reactivity of a Mo₂C substrate with that of metal.^{10,19} In this article, we study the hydrogenation of CO₂ on Cu/Mo₂C(001) surfaces and Cu/Mo₂C powders using a combination of experiment and theoretical models. The addition of Cu to a Mo₂C substrate produces drastic changes in the selectivity of the system towards CH₄ and CH₃OH. The yield of methanol on a Cu/Mo₂C(001) surface is substantially larger than on bare Mo₂C(001), Cu(111) or a Cu/ZnO(000 $\bar{1}$) model for an industrial catalyst.

II. Experimental and theoretical methods

II.1 Sample preparation and tests of catalytic activity

We investigated the performance of Cu/Mo₂C(001) surfaces and Cu/Mo₂C powders for the hydrogenation of CO₂. The experimental data for the Cu/Mo₂C(001) surfaces were collected in a set-up that combined an ultra-high vacuum (UHV) chamber for surface characterization and a micro-reactor for catalytic tests.^{12,14,15} The UHV chamber was equipped with instrumentation for X-ray photoelectron spectroscopy (XPS), low-energy electron diffraction (LEED), ion-scattering spectroscopy (ISS), and thermal-desorption mass spectroscopy (TDS).^{12,14,15}

Ion bombardment and subsequent annealing at 1000 K were used to clean and

prepare the β -Mo₂C(001) surface.¹⁶ Images of scanning tunneling microscopy indicate that, under these conditions, this surface has the expected bulk-terminated (1×1) orthorhombic periodicity,¹⁶ with two or three rotationally misaligned orthorhombic domains. The surface may contain regions with Mo or C termination. Cu was vapor deposited on the Mo₂C(001) substrate at 300 K.¹² In the studies of CO₂ hydrogenation, the sample was transferred to the reactor at ~300 K, then the reactant gases, 0.049 MPa (0.5 atm) of CO₂ and 0.441 MPa (4.5 atm) of H₂, were introduced and the sample was rapidly heated to the reaction temperature (500, 525, 550, 575, and 600 K). This set of pressure and temperature conditions is identical to those used in previous studies for CO₂ hydrogenation on Cu/ZnO(000 $\bar{1}$)²⁰ and ZnO/Cu(111).²¹ Product yields were analyzed by a gas chromatograph.^{12,14,15} In our experiments data was collected at intervals of 15 min up to a total reaction time of 270 min. The amount of molecules (CO, CH₄, or CH₃OH) produced in the catalytic tests was normalized by the active area exposed by the sample and the total reaction time. The kinetic experiments were done in the limit of low conversion (< 5%).

The Cu/Mo₂C powder catalysts were prepared following the methodology described in refs.^{22,23} where Cu₃(MoO₄)₂(OH)₂ and MoO₃ impregnated with 5%wt or 9%wt of Cu were used as catalyst precursors. These precursors were carburized in a flow type fixed bed micro-reactor at elevated temperatures (500 to 950 K ramp) using a gas mixture of 10% methane and 90% hydrogen.²³ X-ray diffraction characterization showed only the expected lines for Cu and β -Mo₂C.^{22,23} Using the Scherrer equation and the main diffraction peak for copper, we estimate average copper particle sizes of < 2 nm for the sample with 5% wt Cu loading, 3.1 nm for the sample with 9%wt Cu loading and 9.3 nm for the sample with 48%wt Cu loading {Cu₃(MoO₄)₂(OH)₂ precursor}. Measurements of

XPS indicate that the copper was in a metallic state and the C/Mo ratio in the catalysts was 0.54-0.57, slightly higher than the one expected for stoichiometric Mo₂C. Thus, the surfaces of the powder catalysts were probably rich in carbon. After the synthesis of the Cu/Mo₂C systems, each sample was directly cooled to the temperatures for CO₂ hydrogenation (473, 523 and 573 K) under a flow of hydrogen and then exposed to a reaction mixture of 10% Ar / 15% CO₂ / 75% H₂, at a flow rate of 30 ml/min, and a total pressure of 2 MPa.^{22,23} The effluent gas from the micro-reactor was analyzed by gas chromatography and mass spectrometry. Under the H₂-rich conditions used in our experiments with the powder catalysts (reaction mixture of 10% Ar / 15% CO₂ / 75% H₂), we did not observe deactivation of the catalysts after 5 h of reaction. Our main objective in this set of experiments was to identify changes in activity and selectivity when going from Mo₂C to Cu/Mo₂C powder catalysts.

II.2 Theoretical methods

The orthorhombic (001) surfaces of Mo carbides (β -Mo₂C(001)-Mo and β -Mo₂C(001)-C) have been represented by appropriate slab models containing four atomic layers, the two outermost layers are relaxed and the two bottommost fixed as in the bulk to provide the appropriate environment to the surfaces layer; this is often referred to as a (2+2) approach. Previous works showed that using thicker slabs leads to structural and energetic properties variations below 5%.²⁴ In all models, a vacuum region with a width larger than 10 Å is added in the direction perpendicular to the surface to avoid the interaction between slabs repeated along the *z* axis direction.

In order to properly represent the experimental systems involving Cu nanoparticles supported on the Mo₂C surfaces several models have been explored as described in recent

work.²⁵ For computational convenience, most of the calculations presented in this work employ a Cu_4 cluster supported on 2×2 unit cell for the Mo- and C-terminated $\text{Mo}_2\text{C}(001)$ surfaces. Nevertheless, larger clusters have been considered to ensure that relevant data do not depend on the choice of this particular model. For the larger clusters a larger 3×3 supercell has been employed. Note that, as previously found for CO adsorption on Mo-terminated $\beta\text{-Mo}_2\text{C}(001)$ surface,¹⁸ the adsorption energy of a reagent, product, or intermediate may vary by more than 1 eV when considering a full saturation coverage, due mostly to lateral interactions. However, Medford *et al.* have recently found that there exists a linear relationship in between moieties adsorbed on this particular surface, *i.e.* the degree of instability is similar for any moiety. Thus, reaction step endo/exothermicity is expected to remain basically unaltered at larger coverages.²⁶ Considering kinetics, note that, in general, TMC follow the Brønsted-Evans-Polanyi (BEP) relationships connecting the reaction step energy barriers with the degree of exothermicity,²⁷ and this BEP relationship has also been found explicitly for the $\beta\text{-Mo}_2\text{C}(001)$ Mo-terminated surface.²⁶

The initial geometry of the naked surfaces and the supported catalyst model of Cu_n deposited on Mo carbide has been taken from previous work²⁵ based on periodic DFT based calculations within the Perdew-Burke-Erzerhof (PBE) implementation of the Generalized Gradient Approach form of the exchange-correlation functional.²⁸ This functional has been found to properly describe Mo carbides²⁴ and provides the best compromise in describing the properties of the bulk of the 30 transition metal elements.^{29,30} The adsorption of species involved in CO_2 hydrogenation and the corresponding sections of the potential energy surface have been studied using the same theoretical approach. Thus, the valence electron density is expanded in a plane-wave basis set with a cut-off of

415 eV for the kinetic energy and the effect caused by the core electrons on the valence region is described by the projector augmented wave method of Blöchl,³¹ as implemented by Kresse and Joubert.³² Integration in the reciprocal space was carried out using $5 \times 5 \times 1$ grids of special k-point within the Monkhorst-Pack³³ scheme. The electronic relaxation was considered converged when the total energy in subsequent iterations varied less than 10^{-5} eV.

Regarding geometry optimization, relaxation of the atomic positions was allowed until forces acting on the atoms are always smaller than $0.01 \text{ eV } \text{Å}^{-1}$. Transition state structures (TS) have been located using the DIMER method.³⁴ Final adsorption minima and TS structures have been characterized *via* frequency analysis. This is carried out by construction and diagonalization of the relevant block of the Hessian matrix whose elements are calculated by finite difference of analytical gradients using individual displacements of 0.03 Å in each cell direction including only elements of the Hessian matrix involving the displacement of atoms in adsorbates are considered.

The adsorption energy, E_{ads} , of an adsorbate X on the naked Mo_2C or Cu_n supported on Mo_2C surfaces, referred generically as *surf*, has been calculated according to:

$$E_{ads} = E_{X/surf} - (E_{surf} + E_X) \quad (1)$$

where $E_{X/surf}$ is the energy of the adsorbate either on the corresponding surface, E_{surf} is the energy of that surface and E_X the energy of the isolated adsorbate. The energy barriers have been computed as usual subtracting the TS energy from that of the reactants. Unless specified all adsorption energy values and energy barriers have been corrected to account for the zero point energy within the harmonic approximation.

All periodic DFT based calculations have been carried out using the Vienna Ab initio Simulation Package (VASP).³⁵

III. Results

III.1 Interaction of CO₂ with Cu/Mo₂C(001) surfaces

Previous studies of XPS have shown that CO₂ dissociates on β -Mo₂C(001) at room temperature to produce CO (531.2-531.5 eV binding energy in the O 1s region) and atomic O (529.8-530.2 eV binding energy) probably bound to Mo sites.¹² The same behavior is observed after dosing CO₂ to a β -Mo₂C(001) surface pre-covered with 0.4 ML of copper, Figure 1. The amount of O present on the surface is larger than that seen for CO. It is known that CO binds well to β -Mo₂C(001).^{12,18} The trends seen in Figure 1 are probably a consequence of the sequential decomposition of CO₂: $\text{CO}_{2,\text{gas}} \rightarrow \text{CO}^* + \text{O}^*$; $\text{CO}^* \rightarrow \text{C}^* + \text{O}^*$ where the * superscript is used to indicate an adsorbed species. We estimate that the maximum coverage of {O* + CO*} in Figure 1 is close to 0.5 of a monolayer. XPS (Cu 2p_{3/2} peak) and Auger (Cu LVV transition) spectra indicated that copper remained in a metallic state after dosing the CO₂. Thus, the surface of the carbide was partially covered by a mixed layer of CO*, O*, and Cu.

In general, the deposition of Cu on β -Mo₂C(001) led to a decrease in the rate of CO₂ dissociation. Figure 2 displays the variation in the O 1s signal for CO after dosing CO₂ to β -Mo₂C(001) and surfaces pre-covered with 0.4 or 0.8 ML of Cu. The larger the coverage of copper present on the carbide surface, the smaller the amount of CO generated by the decomposition of CO₂. This could be a consequence of two different facts. On the one hand, copper does not bind CO well at room temperature under UHV conditions.³⁶⁻³⁸

Thus, any CO deposited on a Cu particle by the reaction $\text{CO}_{2,\text{gas}} \rightarrow \text{CO}^* + \text{O}^*$ will desorb as is corroborated by theoretical calculations detailed in the following sections. On the other hand, as we will discuss in the next section, the data in Figure 2 is consistent with a theoretical result which predicts that CO_2 binds poorly and does not dissociate spontaneously on copper particles deposited on $\text{Mo}_2\text{C}(001)$. The dissociation of C-O bonds on copper is thermodynamically favorable only when assisted by hydrogenation of CO_2 ; for instance *via* $\text{H}^* + \text{CO}_2^* \rightarrow \text{COOH}^* \rightarrow \text{HO}^* + \text{CO}^*$ as a possible mechanism. Without H^* , CO_2^* can decompose to produce CO only on sites of $\beta\text{-Mo}_2\text{C}(001)$ not covered by copper. The oxygen deposited of the carbide surface by the $\text{CO}_{2,\text{gas}} \rightarrow \text{CO}^* + \text{O}^*$ reaction can lead to poisoning.⁵ In order to prevent this, the hydrogenation of CO_2 will be carried out under hydrogen rich conditions.

III.2 Hydrogenation of CO_2 on $\text{Cu}/\text{Mo}_2\text{C}(001)$ surfaces and $\text{Cu}/\text{Mo}_2\text{C}$ powders

The main products for the hydrogenation of CO_2 on a bare $\beta\text{-Mo}_2\text{C}(001)$ surface are CH_4 , CO, and CH_3OH with traces of C_2H_6 , $\text{C}_2\text{H}_5\text{OH}$ and CH_3OCH_3 .¹² The left-side panel in Figure 3 displays an Arrhenius plot for the rates of formation of CH_4 , CO, and CH_3OH on $\beta\text{-Mo}_2\text{C}(001)$. The surface always produces a small amount of methanol. At temperatures between 500 and 575 K, the yields for CO and CH_4 are very close. As the temperature increases, the full decomposition of CO_2 to C and its hydrogenation to CH_4 becomes dominant. The deposition of 0.4 ML of Cu on the $\beta\text{-Mo}_2\text{C}(001)$ surface enhanced the total conversion of CO_2 by 25-35% and completely altered the selectivity of the CO_2 hydrogenation reaction (right-side panel in Figure 3). The production of methane decreased while the generation of CO and CH_3OH increased. It is likely that the Cu present on the surface blocked the full decomposition of CO_2 preventing the poisoning of active sites and

the final formation of CH₄ since limited amounts of C were available on the surface. The DFT based calculations discussed in the next section fully support this interpretation.

We found that the coverage of copper has a strong influence on the performance of the Cu/Mo₂C(001) catalysts. Figure 4 displays the rate for the formation of methanol on a series of Cu/Mo₂C(001) surfaces. At small to medium coverages of Cu there is a constant increase in catalytic activity with a maximum seen around 0.4 ML. At this point we also observed a maximum in the total conversion of CO₂ and the production of CH₃OH. These trends suggest that the Cu-Mo₂C interface and/or particular Cu nanoparticle sizes play a key role in the catalysis. This interface has special properties not seen for isolated Cu or Mo₂C. Figure 5 shows the effects of Cu coverage on the production of methane. The pronounced drop in the rate of methane production supports the idea that Cu is probably blocking the highly active sites that dissociate CO and hydrogenate C to form CH₄. These sites are intrinsically associated with the carbide surface. At copper coverages below 0.4 ML, a Cu-Mo₂C interface is generated that still can adsorb well CO₂ and transform it into CO and methanol. When the copper coverage goes above 0.4 ML, the whole reactivity of the catalytic system drops and we found a drastic decrease in the total conversion of CO₂ and in the formation of CO, CH₄ and CH₃OH.

Figure 6 compares the rates for the production of methanol at 550 K on Cu(111),²⁰ bare β-Mo₂C(001), a carbide surface with 0.4 ML of copper, ZnO/Cu(111)²¹ and a Cu/ZnO(000ī) system, which is a model for an industrial catalyst for methanol synthesis.²⁰ It is known that the way in which a Cu/ZnO catalyst is prepared can have a strong impact in its activity for methanol synthesis.³⁹ In Figure 6, an improvement in the catalytic activity is seen when going from pure Cu(111) to Cu/ZnO(000ī) or ZnO/Cu(111), but by large the

best catalyst is Cu/Mo₂C(001). The amounts of Cu on ZnO(000 $\bar{1}$)²⁰ and β -Mo₂C(001) are similar, but the Cu-ZnO interface seems to be less efficient than the Cu-Mo₂C interface for the CO₂ \rightarrow CH₃OH conversion. The intrinsic ability of Mo₂C to adsorb and dissociate CO₂ probably facilitates the process.

In order to better connect to systems used in practical catalysis, we also investigated the behavior of Cu/Mo₂C powder catalysts. With the caveat that a well-defined β -Mo₂C(001) substrate and powder catalysts may exhibit different surface structural features, Table I summarizes the product distribution for the hydrogenation of CO₂ on these systems at temperatures between 473 and 573 K. As in the case of the experiments with the single crystal, the main products of the reaction are CO, methane and methanol but these catalysts also produced measurable amounts of C₂H₅OH, CH₃OCH₃, C₂H₆ and C₃H₈. So, there is a difference in the nature of the active sites when going from the single crystal to the powder systems. In general, the addition of copper to the β -Mo₂C powder reduces the yield of methane and improves the formation of methanol whereas the amount of CO increases very slightly. (Figure 7 and Table I). The best system is a catalyst that contains 5%wt of Cu. This catalyst exhibited the highest conversion of CO₂ and the biggest production of methanol. An increase in the copper coverage from 5%wt to 9%wt or 48%wt had a negative effect on both properties. The methodology used for the preparation of the Cu/Mo₂C powder catalysts^{22,23} probably generates surfaces which are rich in carbon with a few active sites for the production of methane or methanol. These active sites are blocked or modified by small amounts of copper. The catalytic activity of the Cu/Mo₂C powders correlate with the copper particle size. The average copper particle sizes determined for the Scherrer equation and XRD are < 2 nm for the sample with 5%wt Cu

loading, 3.1 nm for the sample with 9%wt Cu loading and 9.3 nm for the sample with 48%wt Cu loading. Thus, the smaller the Cu particle size, the larger the CO₂ conversion and methanol production in Table 1.

III.3 DFT studies for CO₂ hydrogenation on Cu/Mo₂C(001) surfaces

In order to corroborate the experimental observations and to determine which reaction path is the most probable, we analyzed the adsorption of the different reagents and their hydrogenations and dissociations by means of periodic DFT based calculations. Figure 8 displays the complex underlying reaction network for this hydrogenation process. The many different reaction pathways have been represented using color codes to differentiate the different possible products: hydrocarbons –orange–, aldehydes –blue–, alcohols –yellow–, acids –green–, and carbonates –brown–. All of these different species are interconnected by black and red arrows, which indicate dissociation or hydrogenation process, respectively.

Owing to the fact that the β -Mo₂C (001) single crystal surface contains two possible terminations —C or Mo, hereafter referred to as β -C and β -Mo, respectively—, the experiments are not able to show the specific role of these different surfaces. Using computational models and DFT calculations we are able to clarify the contribution of each different termination to CO₂ hydrogenation. The next subsections show a detailed computational study on clean and Cu supported β -Mo and β -C surfaces, highlight the most probable reaction routes for methanol synthesis and provide arguments to rationalize the experimental observations.

III.3.1 Pristine β -Mo₂C (001) Surfaces

In a first step, CO₂ adsorption and subsequent hydrogenation or dissociation has been studied on the clean β -Mo and β -C surfaces. In the case of the β -Mo surface, CO₂ dissociation is favored over hydrogenation since the energy barrier for CO₂ dissociation is only 0.21 eV whereas the first hydrogenation elementary steps is endothermic by at least 0.25 eV implying an even higher energy barrier. Thereupon, the dominant pathway for the majority of CO₂* will be dissociation towards CO* –see Figure 9–. The reported¹² XPS for the O*(1s) binding energy shows that the amount of atomic O on the surface is superior to the amount of CO* which strongly suggests that CO* dissociation follows the dissociation of CO₂*. This interpretation is in agreement with present theoretical results, where the CO* dissociation entails an energy barrier of 0.86 eV and it is one of the possible elementary steps explaining CH₄ formation ($C+2H_2 \rightarrow CH_4$) *via* the hydrocarbons pathway (orange) represented on Figure 8. However, one needs to keep in mind that the above conclusion regarding CO* formation comes from the β -Mo surface and that CO* is also predicted to be formed on the β -C one as discussed below. Moreover, the O* adatom could form water or could be strongly adsorbed on the surface, poisoning some reactive sites.

On the other hand, CO* could be hydrogenated towards an aldehyde-like intermediate (HCO*) since it is thermodynamically more stable than the alcohol-like species (COH*) and the energy barrier is lower. Nevertheless, HCO* formation is slightly less favorable than CO* dissociation because it involves an energy barrier of 0.99 eV. This difference enhances methane production with respect to methanol, but it is not enough to fully justify the experimental observations –Figure 3, left panel– where the amount of CH₄ is clearly superior to the amount of methanol. Thus, other reaction paths must be

investigated in order to further understand the observed $\text{CH}_4:\text{CH}_3\text{OH}$ ratio production. From Figure 9, it appears that the methoxy intermediate (H_3CO^*) plays a crucial role. Once the HCO^* specie is formed, it could be easily hydrogenated towards H_3CO^* (blue pathway). Although the last hydrogenation to CH_3OH^* implies an energy barrier of 1.28 eV overcoming an energy barrier of 1.22 eV, H_3CO^* could dissociate producing the last intermediate involved in CH_4 production (CH_3^*+O^*). Eventually, the CH_3^* intermediate evolves to methane through a moderate energy barrier (1.05 eV). According to the calculated barriers, the productions of methanol and methane are likely comparable, while the desorption energies of both species play an important role in tuning the selectivity towards methane rather than methanol. Methane desorption occurs readily on the $\beta\text{-Mo}$ termination surface⁴⁰ whereas methanol desorption is less favorable than the reverse dehydrogenation to H_3CO^* , which entails a problematic fact for methanol production, favoring the CH_4 formation in agreement with the experimental results in the left panel of Figure 3.

Regarding the $\beta\text{-C}$ surface, the present DFT calculations show that it is less reactive than the $\beta\text{-Mo}$ one. In fact, CO_2 , H_2 ,⁷ and CO adsorptions are less favorable (exhibiting a lower exothermicity). Figure 10 portrays the CO_2^* dissociation –left– and hydrogenation –right– pathways showing that the $\beta\text{-C}$ surface is a CO^* generator because it is able to dissociate CO_2^* towards CO^* as in the Mo terminated surface with an energy barrier of 0.48 eV. However, the formed CO^* is hardly further promoted towards dissociation or hydrogenation, since the energy barriers are both higher than 1.4 eV. In addition, CO_2^* could be hydrogenated towards carboxylate specie (COOH^*) with an energy barrier of 0.64 eV, although calculations show that this intermediate readily dissociates into CO^* and

OH* through a small energy barrier of 0.59 eV. Further hydrogenation towards formic acid (green pathway) is also discarded since it involves a large energy barrier (>2 eV). On the other hand, the atomic oxygen released in the CO₂* dissociation step is strongly adsorbed on both β -Mo and β -C surfaces. In this sense it is important to point out that O adsorption on the β -C surface could entail CO* formation through bonding to C surface atoms as predicted by Liu and Rodriguez.⁴¹ This possibility could imply a new way for CO production and the generation of new Mo terminated surfaces, which catalyze the methanol and methane synthesis as we explain above.

Note that methanol synthesis is not the final point during the reaction, but that the oxygen formed during CO formation would hydrogenate together with an extra H₂ molecule to water. The water formation reaction steps are slightly endothermic, and the final H₂O desorption requires 0.65 eV according to present DFT calculations, thus not being a rate limiting step, and so, presence of water is not a reaction inhibitor. Note also by passing by that the reaction enthalpy of -0.43 eV is close to the experimental value of \sim -0.5 eV.^{42,43}

In summary, methanol is produced *via* CO* hydrogenation on the β -Mo surface, although during the synthesis, this route competes at least against two different methane production paths, CO* and H₃CO* dissociation, which are slightly favorable processes. These results, added to the handicap of the methanol desorption energy, explain the limited capability of the β -Mo surface to produce methanol since, at the same time, it becomes a CH₄ generator. Note that at high temperatures this is the main product, even above the production of CO, which is formed on both terminations of the β -Mo₂C(001) surface.

III.3.2 Cu/ β -Mo₂C (001) surface models

In a previous study,²⁵ theoretical models of Cu supported clusters were reported showing that Cu_n clusters in contact with β -Mo₂C(001) adopt a planar configuration, independently of the surface termination. In the present work, the study the mechanism of methanol synthesis have been performed using Cu₄ cluster models supported on β -Mo₂C(001) with Mo or C termination. The justification for this choice is twofold. On the one hand, the Cu₄, Cu₇, or Cu₁₀ clusters supported on the β -Mo surface exhibit a very similar energy profile for CO₂ adsorption and dissociation (Figure 11) and, on the other hand, the use of larger clusters implies a larger supercell and the overall computational resources required are excessive. Moreover, the interaction of CO₂ with the supported Cu clusters is weak, and subsequently the dissociation energy barrier is much higher than the desorption energy (Figure 11), in agreement with the experimental results in Figure 2 which show that the amount of detected CO* decreases when the Cu coverage increases. Indeed, CO₂ adsorption energy values –see Table 2– are larger for the clean β -Mo and β -C surfaces (-1.38 and -0.61 eV respectively) than on the Cu adclusters (-0.14 and -0.06 eV respectively). Thus, as is suggested by experiments, the CO₂ conversion on Cu adclusters must be assisted by hydrogen implying a different molecular mechanism as well.

One can properly argue that the Cu₄/ β -Mo₂C surface models provide an oversimplified representation of the real systems. Therefore, the main aim of this part is to find the main trends. The main goal here is to contribute and to clear up the experimental results, such as the selectivity switch between CH₄ and CH₃OH or the enhancement in the reactivity of Cu/ β -Mo₂C (001) systems with respect to the bare surfaces, taking into account that the number of possible reaction pathways and intermediates is excessively

large. We will present compelling evidence that this simplified model explain most of the experimental observations.

Next, we describe in detail the results obtained for CO₂ hydrogenation on Cu₄/β-Mo₂C (001) surfaces. It has been already commented that the Mo terminated surface is much more reactive towards CO₂ dissociation than the C-terminated one; this tendency follows even after Cu deposition. Figure 12 presents two different reaction paths for CO₂ hydrogenation on the Cu₄/β-Mo surface model. This figure shows the most probable ways for CH₃OH (Figure 12a) and CO (Figure 12b) production, chosen from all different possibilities screened because they present the lowest energy barriers. Interestingly, these energy profiles, including forward and reverse reactions, account for most of the experimental observations and strongly suggest that the methanol route (Figure 12a) is dominant as explained in detail below. Alternative, less likely, pathways are reported in Figure S1 in the supporting information. These include those reported in previous works for CO₂ hydrogenation using models for Cu as catalyst, either in the form of extended surfaces, clusters models, or Cu supported clusters.⁴⁴⁻⁴⁷

Methanol production, as predicted by the Cu₄/β-Mo model, entails the formation of a formate species (HCOO*), which is the most stable reaction intermediate. The other possible intermediate, the carboxyl species (COOH*) is ~1 eV less stable than HCOO*. However, in spite of being thermodynamically less favored it could be formed on the interface between Cu and a Mo terminated surface with slightly lower energy barrier than HCOO*. Oftentimes, the rate limiting step for methanol synthesis is precisely the evolution from HCOO* to H₃CO* species.⁴⁸ Considering that the HCO* intermediate is not very stable on Cu clusters and that the HCOO* dissociation barrier is larger than 2.5

eV, HCOO* hydrogenation towards dioxymethylene (H₂COO*) or formic acid (HCOOH*) appears as alternative route where both intermediates evolve to H₂CO*, and eventually it hydrogenates to CH₃OH. Indeed, the present calculations on the Cu₄/β-Mo model suggest that the route towards CH₃OH production implies the H₂COO* formation (Figure 12a), in agreement with several works on related Cu surfaces.^{49,50} This assertion follows from the DFT calculations showing that H₂COO* is more stable than HCOOH* on Cu supported clusters (~0.5 eV) and that the HCOO*→HCOOH* process entails an energy barrier of 1.26 eV (see SI) above the Cu₄ supported cluster, implying that HCOOH* does not form on the Cu-Mo carbide interface. In addition, despite the fact that the energy barrier leading to H₂COO* is similar to that leading to HCOOH* on top of Cu₄ supported cluster, the calculated energy barrier for H₂COO* formation at the Cu-Mo₂C interface is 0.61 eV which under reaction conditions should not be an impediment. Moreover, as is displayed in Figure S1, given that HCOOH would be formed, it would rather react back to HCOO* than desorb, see below. Indeed, the only exit for HCOO* would be do reverse react towards CO₂ + H₂ through a competitive reaction step energy barrier. Note as well that CO₂ + 2H₂ energy level is located below HCOOH, strengthening the thermodynamics of the process. Also, would some HCOOH* be formed, it will easily desorb (0.45 eV, Table 2) and hence, further hydrogenation towards the H₂COOH* intermediate cannot occur. Nevertheless, HCOOH* has not been detected in the experiments, not even in trace amounts. Therefore, taking into account the available information it can be safely concluded that HCOOH* is not a key path as suggested by Taylor *et al.*⁵¹ and that HCOO* hydrogenation leads to a H₂COO* intermediate as in the pathway schematically shown in Figure 12a.

The next step towards methanol involves H₃CO* formation *via* H₂COO*

hydrogenation as already proposed in some kinetic models.^{52,53} However Grabow and Mavrikakis suggest instead that H_2COO^* dissociates to $\text{H}_2\text{CO}^* + \text{O}^*$ and that H_2CO^* is subsequently hydrogenated to H_3CO^* .⁴⁴ Note, however, that H_2CO^* can either occupy sites involving the clean surface or the supported Cu cluster region. For the former, H_2CO^* hydrogenation will follow the reaction pathway discussed above (Figure 9) where methane formation is favored with respect to methanol. Here it is worth realizing that the deposition of Cu clusters decreases the number of reactive sites for CH_4 production on the clean region which is in agreement with the experimental results in Figure 5. In this sense, one can speculate that methanol formation is enhanced by migration of part of the formed H_2CO^* to the supported Cu cluster where further hydrogenation towards a methoxy intermediate would be possible. Above the supported cluster the energy barrier for H_3CO^* dissociation into CH_3^* and O^* is higher than 2 eV whilst hydrogenation of H_3CO^* to CH_3OH^* is of only 1.23 eV — virtually, the same energy barrier as for H_3CO^* hydrogenation on a clean β -Mo surface. Hydrogenation of H_3CO^* to methanol is favored with respect to dissociation eventually leading to CH_4 which, again, is in agreement with the experimental observations. Furthermore, the CH_3OH^* desorption on Cu_4 clusters is a favorable process, contrary to CH_3OH^* desorption on naked regions. The results discussed above probably contain one of the keys to explain the selectivity switch between methane and methanol detected on the experiments –see Figure 3, right panel.

We devote now our attention to the CO production pathway which is less likely because of the competition between forward and reverse steps. Here COOH^* is the key intermediate (Figure 12b) since dissociation into CO^* and OH^* is extremely favorable involving an energy barrier of only 0.19 eV. Note that CO^* hydrogenation or dissociation

on Cu₄ supported clusters are prohibitive steps involving energy barriers higher than 2 eV. Therefore, the supported Cu clusters avoid CO dissociation and the subsequent reaction towards CH₄ (orange way) which adds one more justification to the selectivity switch from CH₄ to CH₃OH production on Cu/Mo₂C relative to Mo₂C as shown in the experiments.

Regarding Cu clusters supported on β-C, where the Cu₄ deposition is slightly favorable respect β-Mo,²⁵ CO₂ direct decomposition is not favored and hydrogenation towards a HCOO* intermediate seems to be more likely. Nevertheless, contrary to the β-Mo surface, a H₂COO* species has not been found in the calculations since all attempts lead to HCOOH* formation with an energy barrier of 1.31 eV and with an adsorption energy slightly stronger than that calculated for the Cu₄/β-Mo models (Table 2). Moreover, HCOOH* hydrogenation to H₂COOH* competes with HCOOH* desorption. The low desorption energy of formic acid together to the absence this product in the experiments strongly suggest that this route can be discarded for the Cu₄/β-C model. Furthermore, the studies carried out on the interface do not show an improvement respect to a clean region surface. In fact, the CO₂ dissociation on C atoms in the neighborhood of a Cu cluster presents an energy barrier slightly superior (0.69 eV) respect to a clean region in the surface. On the other hand, the role of the Cu₄/β-C surface in the catalytic process could be similar to that of a clean region; despite of the Cu deposition, CO* formation from the bonding between an O* adatom and a C surface atom is not affected. Therefore, the CO produced could desorb, leading to a Mo layer-Cu cluster interaction, which could entail the same reactivity explained above.

Conclusions

Here, a combined experimental and theoretical study has been presented regarding CO₂ hydrogenation on the bare orthorhombic (001) surfaces of Mo₂C, including the two possible terminations on Mo or C atoms, and on Cu clusters supported thereon.

Experiments carried out for the clean surface involve simultaneously the Mo- and C-terminated surfaces; results show that CO₂ is activated and dissociated, leading to CH₄ and CO as main products but also to a noticeable amount of CH₃OH. Periodic DFT calculations clearly show that CH₃OH, CH₄, and CO formation takes place on the Mo-terminated surface *via* CO₂ dissociation. Furthermore, the different selectivity towards CH₄ and CH₃OH is explained since methanol production (*via* CO* hydrogenation) competes with, at least, two different reaction pathways leading to methane formation (CO* and H₃CO* dissociation) which are slightly more favorable, thus explaining the origin of the experimental results. Besides, CH₃OH* desorption is unfavorable since dehydrogenation implies a smaller energy barrier. On the other hand, DFT calculations show that the C-terminated surface acts as a CO generator through three main routes: direct CO₂ dissociation, through CO₂* hydrogenation to COOH* and subsequent dissociation into CO* and OH* and through reaction between O* and surface C atoms which in turn increases the area of the Mo-terminated surface.

For the Cu/Mo₂C systems, the experimental results show that, relative to the bare Mo₂C surfaces, CO₂ conversion increases by about 25-35%. Furthermore, experimental observations reveal a selectivity switch between CH₃OH and CH₄, a decrease of methane and an increase in the amount of methanol. This is interpreted in terms of Cu blocking the most reactive surface sites involved in CH₄ production. Periodic DFT calculations carried

out on a $\text{Cu}_4/\text{Mo}_2\text{C}$ model disclosed some of the reasons behind this change of selectivity. First, the DFT calculations suggest a possible new route for methanol production involving the formation of a HCOO^* intermediate which is subsequently hydrogenated to H_2COO^* at the interface formed by Mo carbide and Cu supported cluster and ultimately leading to CH_3O^* and to CH_3OH . Besides, on the supported Cu surface model, methoxy dissociation, necessary to produce methane, is not favorable whereas methanol desorption is a favorable process, justifying the selectivity switch observed in the experiments. Also, the DFT calculations predict that the supported Cu clusters are not able to dissociate CO^* , eventually produced through COOH^* dissociation, thus explaining the observation that under Cu deposition on Mo_2C , the amount of methane decreases.

In summary, deposition of Cu on Mo_2C results in an increase in the CO_2 conversion under the presence of H_2 and also in an increase of CH_3OH and a decrease of CH_4 . Experiments carried out on $\text{Cu}/\text{Mo}_2\text{C}(001)$ well defined systems and on $\text{Cu}/\text{Mo}_2\text{C}$ powders complemented by periodic DFT calculations on suitable models have determined the different roles of the supported Cu cluster on CO_2 hydrogenation. These are *i*) to block the clean region sites for CH_4 production, *ii*) to generate a new route for CH_3OH production involving sites at the Cu- Mo_2C interface, increasing selectivity towards methanol *iii*) to hinder CO^* and H_3CO^* dissociation thus leading to a decrease of CH_4 and *iv*) to favor the CH_3OH desorption.

Acknowledgments

This manuscript has been authored by employees of Brookhaven Science Associates, LLC under Contract No. DE-SC0012704 with the U.S. Department of Energy. The research carried out at the *Universitat de Barcelona* was supported by the Spanish MINECO grant CTQ2012-30751 grant and, in part, by *Generalitat de Catalunya* (grants 2014SGR97 and XRQTC). S.P.P. acknowledges financial support from Spanish MEC predoctoral grant associated to CTQ2012-30751 and F.V. thanks the MINECO for a postdoctoral *Ramón y Cajal* (RyC) research contract (RYC-2012-10129). Computational time at the *MARENOSTRUM* supercomputer has been provided by the Barcelona Supercomputing Centre (BSC) through a grant from *Red Española de Supercomputación* (RES).

Table 1. CO₂ Hydrogenation over β -Mo₂C and Cu/ β -Mo₂C powder catalysts ^a

Catalyst	Temp. (K)	CO ₂ conv(%)	Selectivity (%)							
			CO	CH ₃ OH	C ₂ H ₅ OH	CH ₃ OCH ₃	CH ₄	C ₂ H ₆	C ₃ H ₈	Others
β -Mo ₂ C	473	6	39	21	1	2	29	5	2	1
	523	17	34	12	0	1	37	9	4	3
	573	24	28	4	0	0	45	13	9	1
Cu/Mo ₂ C (5%wt Cu)	473	9	41	42	1	1	11	1	1	2
	523	21	38	31	1	2	20	3	2	3
	573	28	35	26	0	1	27	5	4	2
Cu/Mo ₂ C (9%wt Cu)	473	7	42	37	1	1	15	1	1	2
	523	19	38	26	2	1	25	3	3	2
	573	26	37	23	1	1	28	5	3	2
Cu/Mo ₂ C ^b (48%wtCu)	473	4	44	34	1	1	16	1	1	2
	523	13	40	21	1	2	28	4	2	2
	573	19	38	17	0	1	32	6	4	2

^a Pressure = 2 MPa; flow rate = 30 ml/min; reaction mixture of Ar/CO₂/H₂ = 10 % / 15 % / 75%.

^b Cu₃(MoO₄)₂(OH)₂ was used as a precursor in the carburization process (from ref. 23).

Table 2: Adsorption energy (eV) of different intermediates on the two possible terminations of β -Mo₂C and Cu₄/ β -Mo₂C.

	CO₂	CO	HCOOH	CH₄	CH₃OH
β-Mo	-1.38	-2.25	<i>NF</i>	-0.1	-0.77
Cu/β-Mo	-0.14	-1.14	-0.45	<i>NF</i>	-0.69
β-C	-0.61	-1.93	<i>NF</i>	-0.05	<i>NF</i>
Cu/β-C	-0.06	-1.22	-0.53	<i>NF</i>	-0.70

NF = Species not formed

Figure 1: Uptake of O and CO after several doses of CO₂ at 300 K to a β -Mo₂C(001) surface pre-covered with 0.4 ML of copper.

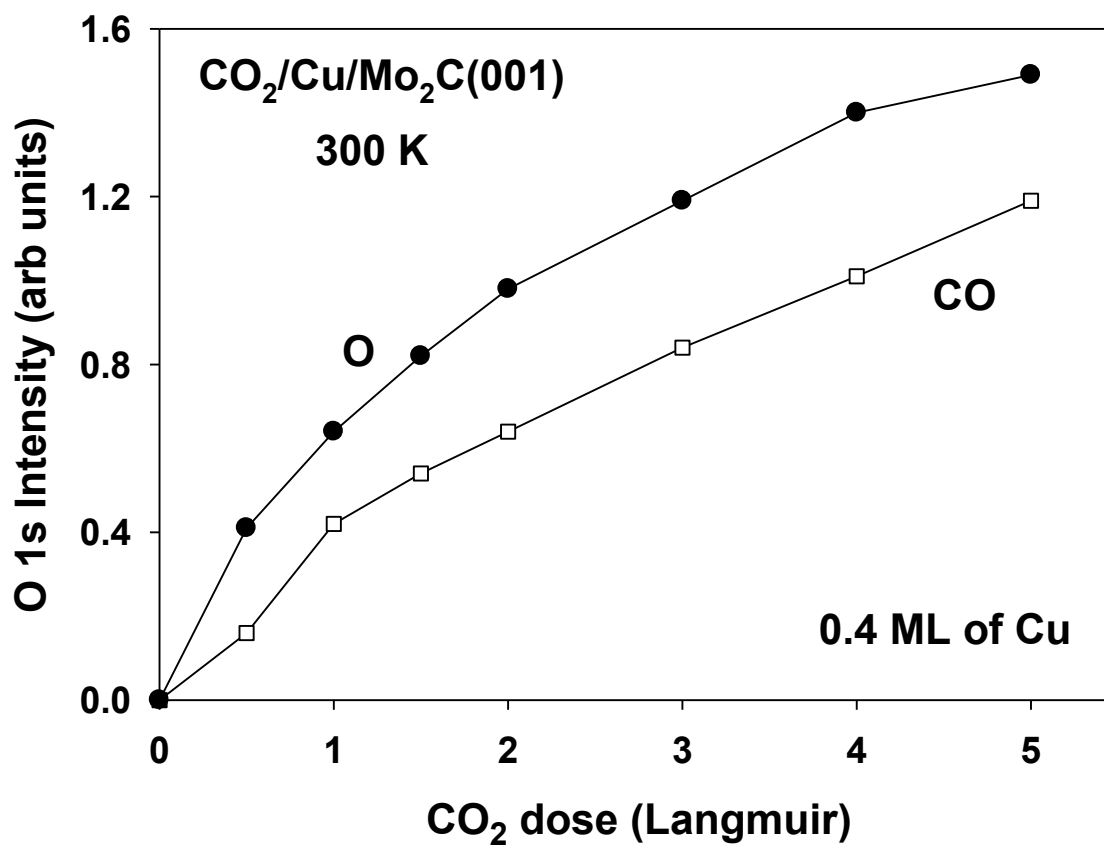


Figure 2: Variation of the O 1s signal for adsorbed CO after several doses of CO₂ to pure β -Mo₂C(001) and surfaces pre-covered with 0.4 or 0.8 ML of copper. T= 300 K.

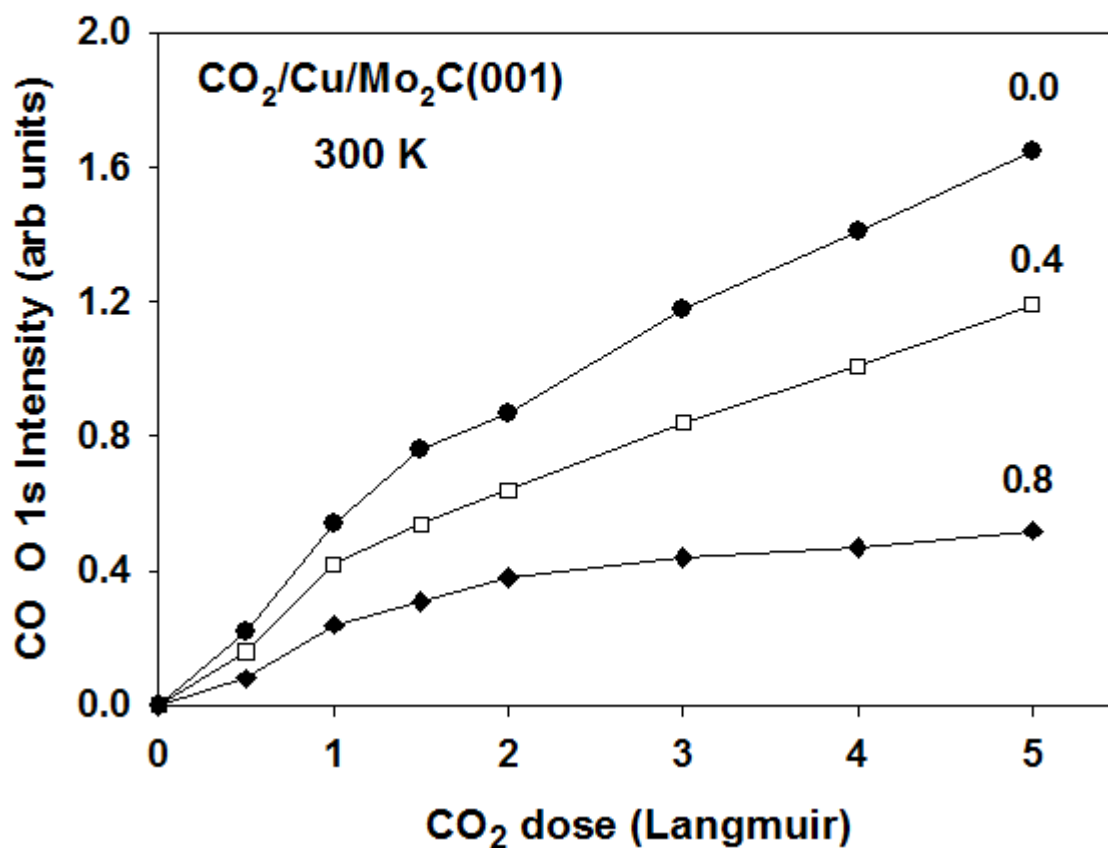


Figure 3: Arrhenius plots for the production of CO, methane and methanol on bare β - $\text{Mo}_2\text{C}(001)$, left-side panel, and a surface pre-covered with 0.4 ML of copper, right-side panel. In a batch reactor, the catalysts were exposed to 0.049 MPa (0.5 atm) of CO_2 and 0.441 MPa (4.5 atm) of H_2 at temperatures of 600, 575, 550, 525 and 500 K.

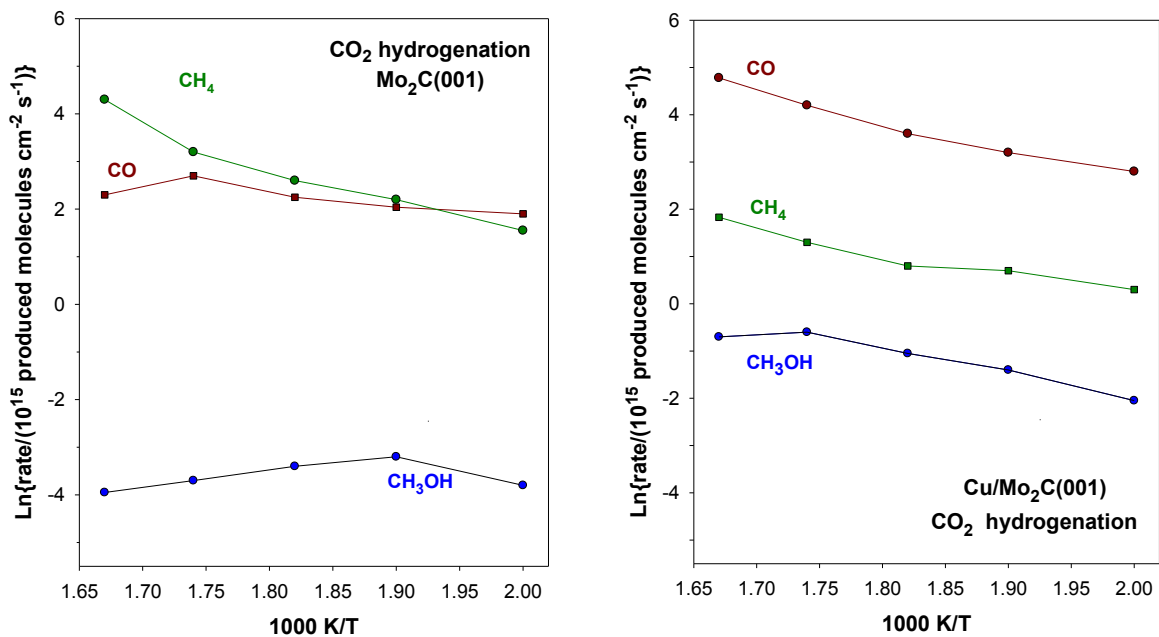


Figure 4: Rate for the production of methanol on Cu/Mo₂C(001) surfaces as a function of copper coverage. In a batch reactor, the catalysts were exposed to 0.049 MPa (0.5 atm) of CO₂ and 0.441 MPa (4.5 atm) of H₂ at a temperature of 550 K.

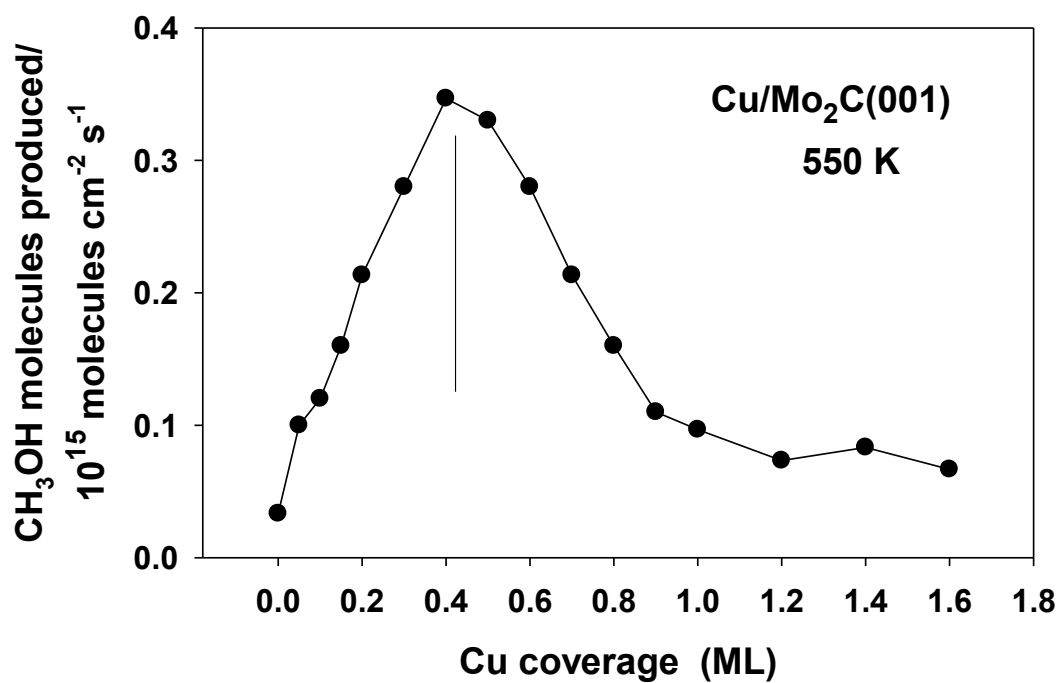


Figure 5: Rate for the production of methane on Cu/Mo₂C(001) surfaces as a function of copper coverage. In a batch reactor, the catalysts were exposed to 0.049 MPa (0.5 atm) of CO₂ and 0.441 MPa (4.5 atm) of H₂ at a temperature of 550 K.

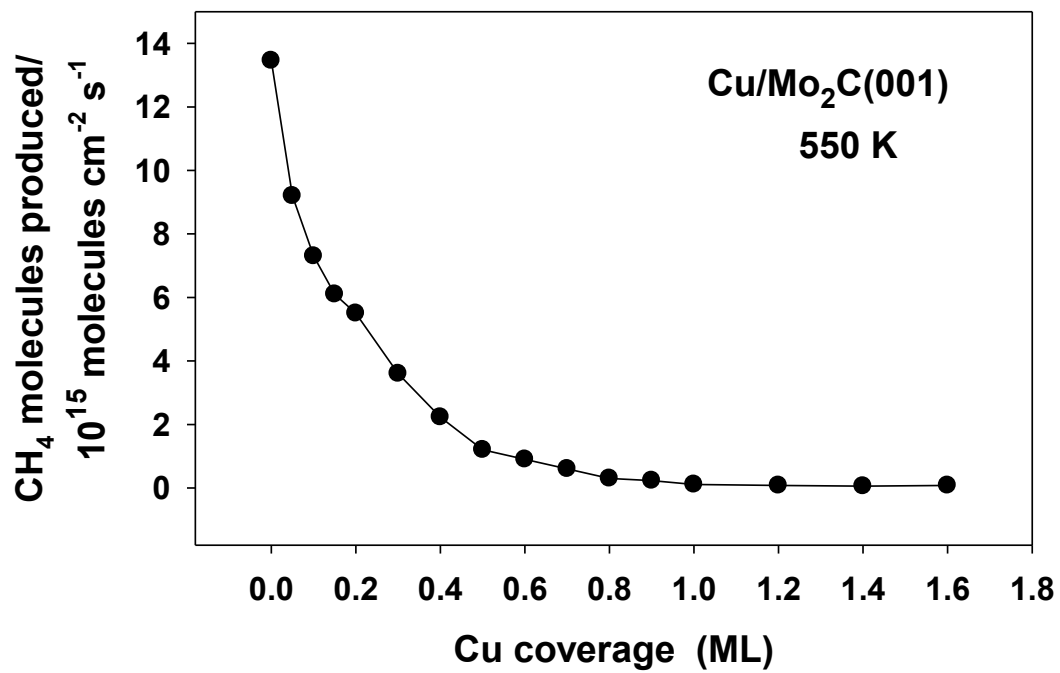


Figure 6: Rates for the production of methanol on Cu(111),²⁰ Cu/ZnO(000 $\bar{1}$),²⁰ ZnO/Cu(111),²¹ bare β -Mo₂C(001) and Cu/Mo₂C(001). In a batch reactor, the catalysts were exposed to 0.049 MPa (0.5 atm) of CO₂ and 0.441 MPa (4.5 atm) of H₂ at a temperature of 550 K.

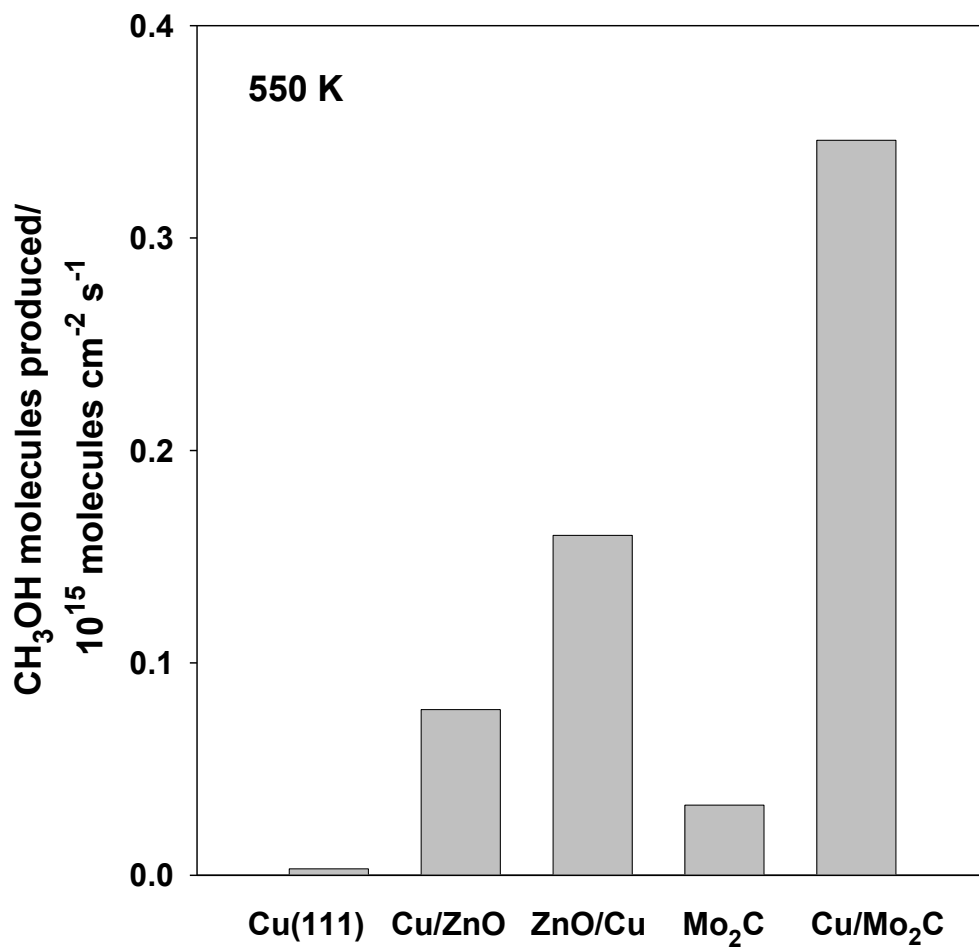


Figure 7: Selectivity for the generation of methanol and methane from CO₂ hydrogenation on β-Mo₂C and on a series of catalysts with different loadings of copper. Total pressure= 2 MPa; flow rate = 30 ml/min; reaction mixture of Ar/CO₂/H₂ = 10% / 15% / 75%.

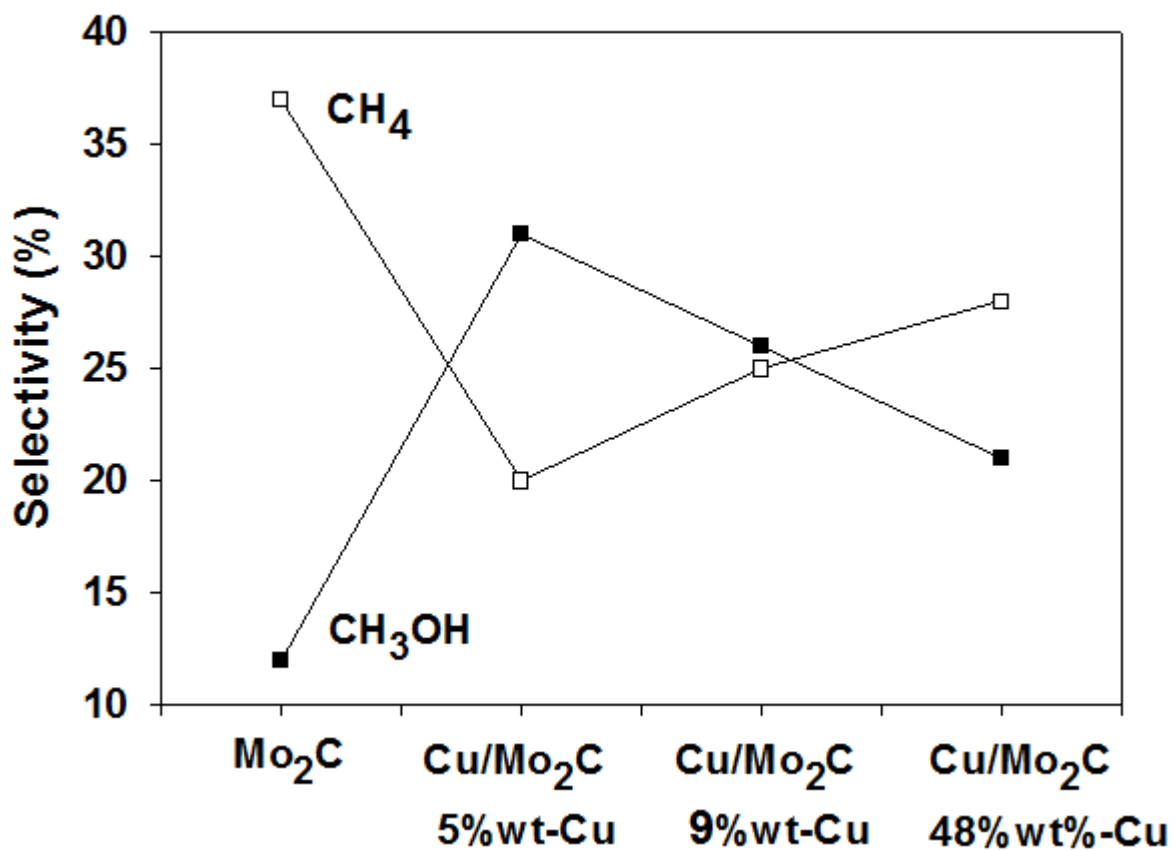


Figure 8: Scheme of the reaction network for the heterogeneously catalyzed CO₂ hydrogenation. Possible reaction intermediates are highlighted using color codes to differentiate the hydrocarbons –orange–, aldehydes –blue–, alcohols –yellow–, acids –green–, and carbonates –brown–.

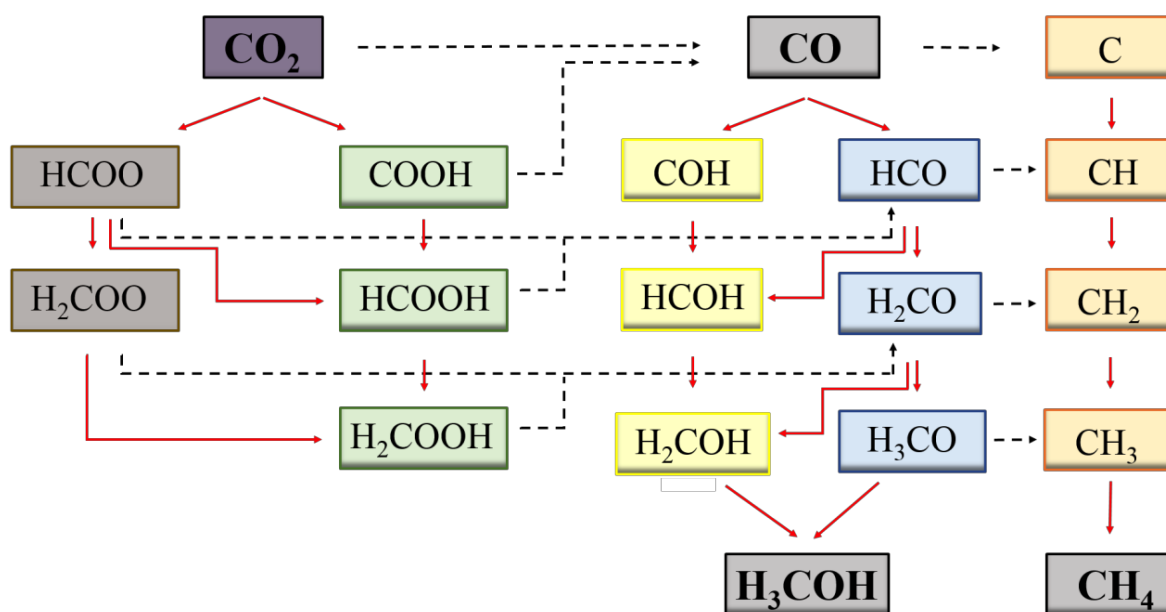


Figure 9: Calculated energy profile for CO₂ hydrogenation on the clean β -Mo₂C(001)-Mo surface. The energy barrier lines follow the reaction paths listed on Figure 8. Purple, green, red and white balls denote Mo, C, O and H atoms respectively.

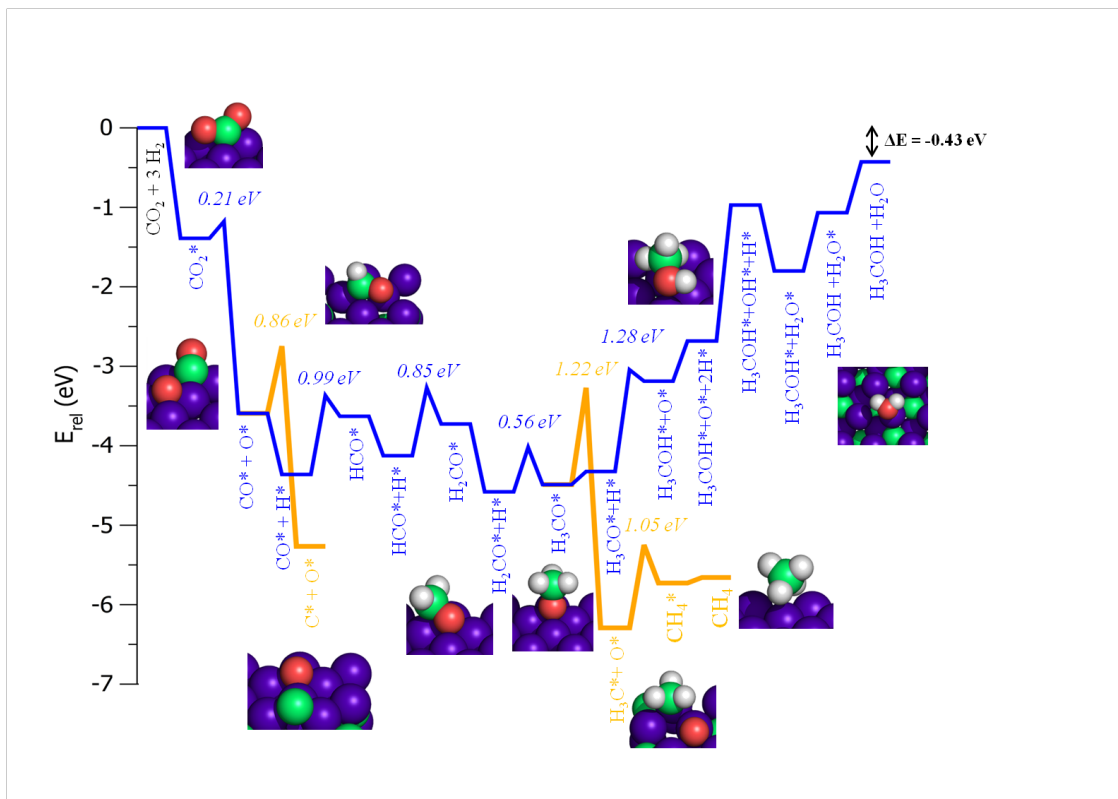


Figure 10: Energy profile of CO₂ dissociation (left) and hydrogenation (right) on clean β-Mo₂C(001)-C surface. The energy barrier lines are in agreement with reaction paths listed on Figure 8. Color code as in Figure 9.

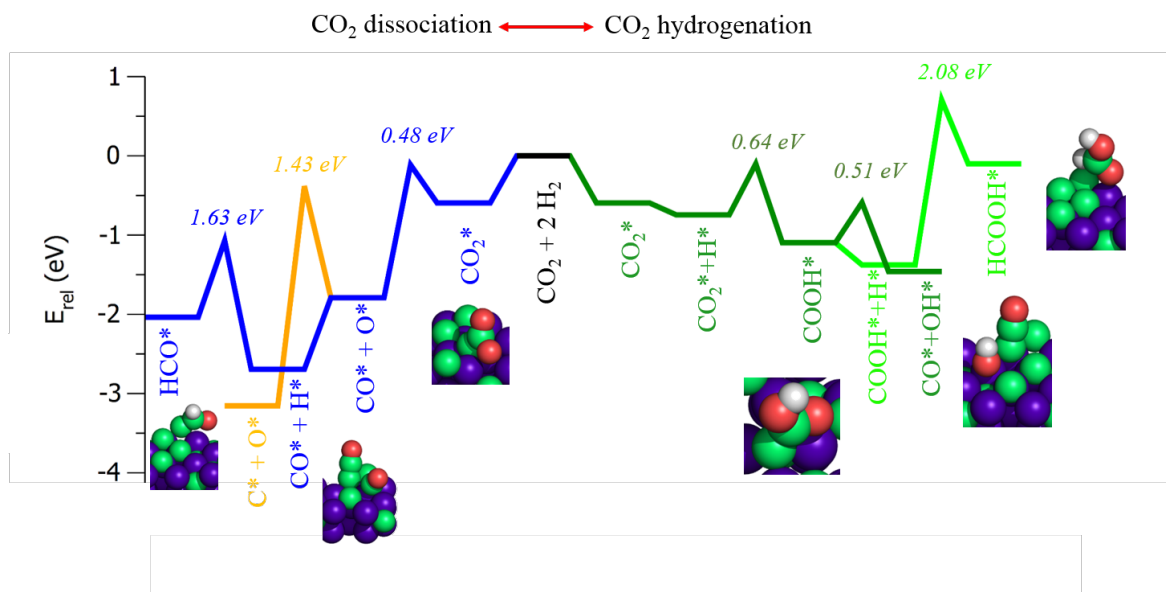


Figure 11: Energy profile for CO₂ dissociation on the clean Mo- and C-terminated surfaces of β -Mo₂C(001) and on various Cu_n/ β -Mo₂C(001) (n=4,7,10) surfaces models.

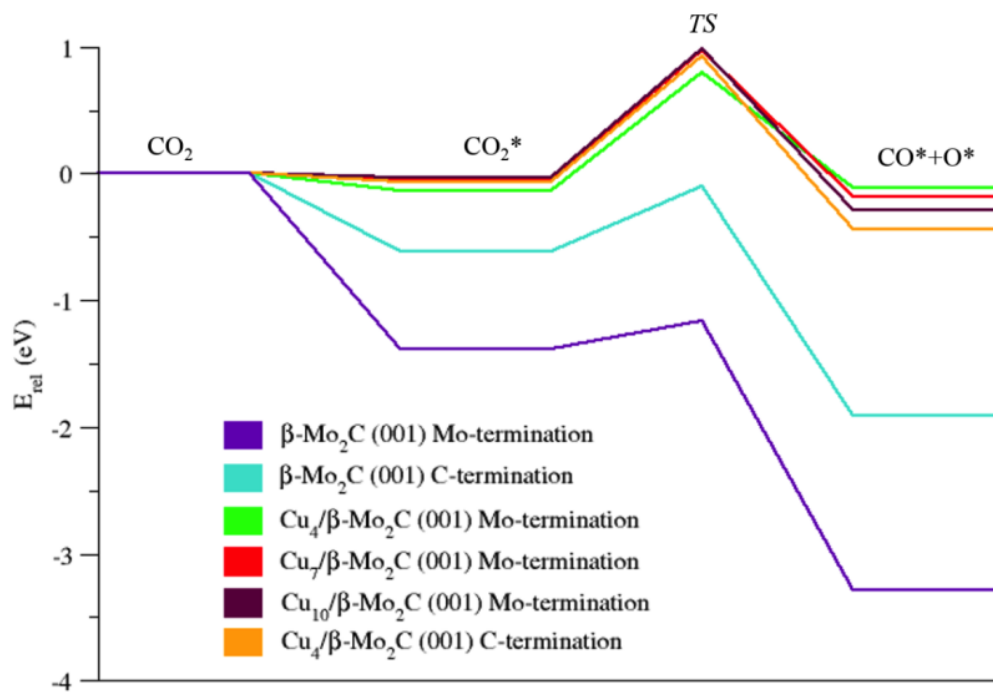
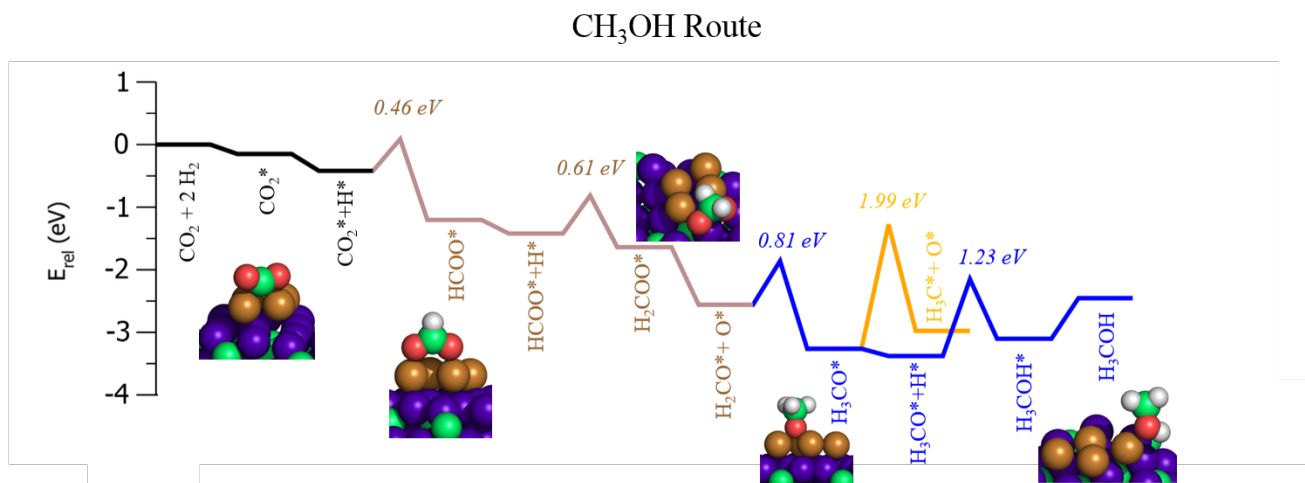
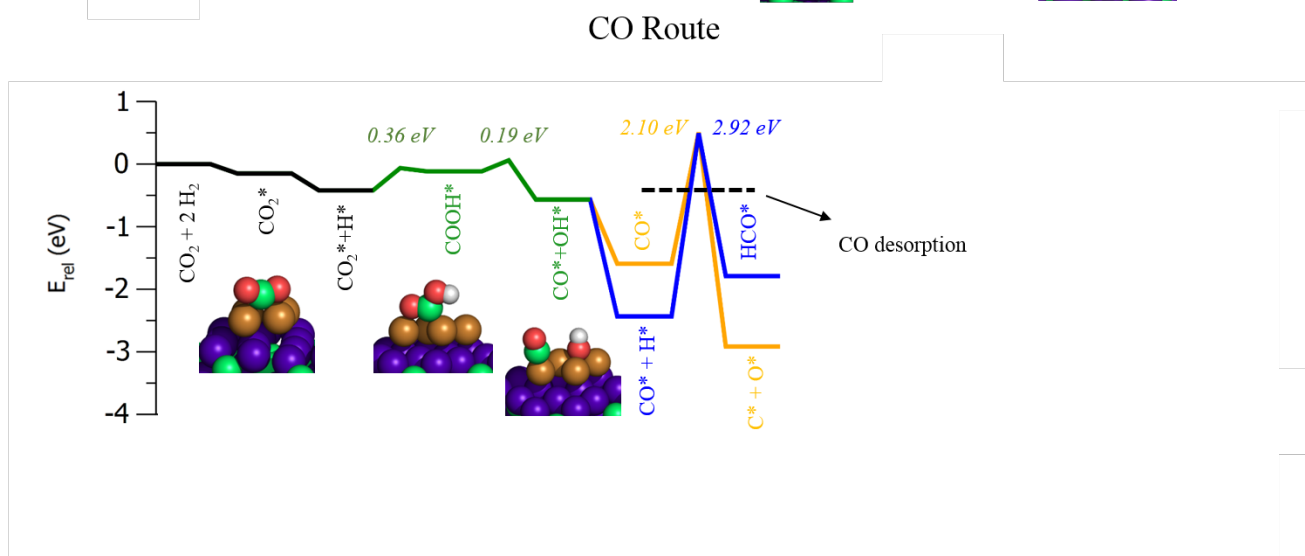


Figure 12: Energy profile of methanol (a) and CO (b) production as predicted from a $\text{Cu}_4/\beta\text{-Mo}$ surface model. Color code as in Figure 9, including the brown balls, which denote Cu atoms.

a)



b)



References

- (1) T. R. Karl and K. E. Trenberth, *Science*, 2003, **302**, 1719.
- (2) X. Lim, *Nature*, 2015, **526**, 628.
- (3) J. A. Rodriguez, P. Liu, D. J. Stacchiola, S. D. Senanayake, M. White and J. G. Chen, *ACS Catal.*, 2015, **5**, 6696.
- (4) *Chemistry of Transition Metal Carbides and Nitrides*, Oyama, S.T. (editor), Springer, Berlin, 1996.
- (5) M. D. Porosoff, S. Kattel, W. Li, P. Liu and J. G. Chen, *Chem. Commun.*, 2015, **51**, 6988.
- (6) J.-L. Dubois, K. Sayama and H. Arakawa, *Chemistry Letters*, 1992, **7**, 1115.
- (7) S. Posada-Pérez, F. Viñes, J. A. Rodriguez and F. Illas, *Top. Catal.*, 2015, **58**, 159.
- (8) S. Wannakao, N. Artrith, J. Limtrakul and A. Kolpak, *ChemSusChem.*, 2015, **8**, 2745.
- (9) F. Solymosi, A. Oszkó, T. Bánsági and P. Tolmácsóv, *J. Phys. Chem. B*, 2002, **106**, 9613.
- (10) M. D. Porosoff, X. Yang, J. A. Boscoboinik and J.G. Chen, *Angew. Chem. Int. Ed.*, 2014, **53**, 6705.
- (11) J. A. Rodriguez and F. Illas, *Phys. Chem. Chem. Phys.*, 2012, **14**, 427.
- (12) S. Posada-Pérez, F. Viñes, P. J. Ramirez, A. B. Vidal, J. A. Rodriguez and F. Illas, *Phys. Chem. Chem. Phys.*, 2014, **16**, 14912.
- (13) A. L. Stottlemyer, T. G. Kelly, Q. Meng and J. G. Chen, *Surf. Sci. Rep.*, 2012, **67**, 201.
- (14) A. B. Vidal, L. Feria, J. Evans, Y. Takahashi, P. Liu, K. Nakamura, F. Illas and J. A. Rodriguez, *J. Phys. Chem. Lett.*, 2012, **3**, 2275.
- (15) J. A. Rodriguez, J. Evans, L. Feria, A. B. Vidal, P. Liu, K. Nakamura and F. Illas, *J. Catal.*, **2013**, *307*, 162.

-
- (16) T. P. Saint Clair, S. T. Oyama, D. F. Cox, S. Otani, Y. Ishizawa, R. L. Low, K. Fukui and Y. Iwasawa, *Surf. Sci.*, 1999, **426**, 187.
- (17) P. Liu, J. A. Rodriguez, T. Asakura, J. Gomes and K. Nakamura, *J. Phys. Chem. B*, 2005, **109**, 4575.
- (18) T. Wang, Y. W. Li, J. Wang, M. Beller and H. Jiao, *J. Phys. Chem. C*, 2014, **118**, 3162.
- (19) N. M. Schweitzer, J. A. Schaidle, O. K. Ezekoye, X. Pan, S. Linic and L. T. Thompson, *J. Am. Chem. Soc.*, 2011, **133**, 2378.
- (20) Y. Yang, J. Evans, J. A. Rodriguez, M. G. White and P. Liu, *Phys. Chem. Chem. Phys.*, 2010, **12**, 9909.
- (21) S. Senanayake, P. J. Ramirez, I. Waluyo, S. Kundu, K. Mudiyansele, Z.-Y. Liu, Z. Liu, S. Axnanda, D. J. Stacchiola, J. Evans and J. A. Rodriguez, *J. Phys. Chem. C*, 2016, **120**, DOI:10.1021/acs.jpcc.5b12012.
- (22) W. Xu, P. J. Ramirez, D. J. Stacchiola and J. A. Rodriguez, *Catal. Lett.*, 2014, 144, 1418.
- (23) W. Xu, P. J. Ramirez, D. J. Stacchiola, J. L. Brito, J. A. Rodriguez, *Catal. Lett.*, 2015, **145**, 1365.
- (24) J. R. d. S. Politi, F. Viñes, J. A. Rodriguez and F. Illas, *Phys. Chem. Chem. Phys.*, 2013, **15**, 12617.
- (25) S. Posada-Pérez, F. Viñes, J. A. Rodriguez and F. Illas, *J. Chem. Phys.*, 2015, **143**, 114704.
- (26) A. J. Medford, A. Vojvodic, F. Studt, F. Abil-Pedersen and J. K. Nørskov, *J. Catal.*, 2012, **290**, 108
- (27) F. Viñes, A. Vojvodic, F. Abil-Pedersen and F. Illas, *J. Phys. Chem. C*, 2013, **117**, 4168.
- (28) J. P. Perdew, K. Burke and M. Ernzerhof, *Phys. Rev. Lett.*, 1996, **77**, 3865.

-
- (29) J. Janthon, S. M. Kozlov, F. Viñes, J. Limtrakul and F. Illas, *J. Chem. Theory Comput.*, 2013, **9**, 1631.
- (30) J. Janthon, S. J. Luo, S. M. Kozlov, F. Viñes, J. Limtrakul, D. G. Trulhar and F. Illas, *J. Chem. Theory Comput.*, 2014, **10**, 3832.
- (31) P. E. Blöchl, *Phys. Rev. B: Condens. Matter Mater. Phys.*, 1994, **50**, 17953.
- (32) G. Kresse and D. Joubert, *Phys. Rev. B: Condens. Matter Mater. Phys.*, 1999, **59**, 1758.
- (33) H. J. Monkhorst and J. D. Pack, *Phys. Rev. B: Solid State*, 1976, **13**, 5188.
- (34) G. Henkelman and H. Jonsson, *J. Chem. Phys.*, 1999, **111**, 7010.
- (35) G. Kresse and J. Furthmüller, *Phys. Rev. B: Condens. Matter Mater. Phys.*, 1996, **54**, 11169.
- (36) M. Gajdoš and J. Hafner, *Surf. Sci.*, 2005, **590**, 117.
- (37) S. Vollmer, C. Witte and C. Woell, *Catal. Lett.*, 2001, **77**, 97.
- (38) J. C. Tracy, *J. Chem. Phys.*, 1972, **56**, 2748.
- (39) M. Kurtz, N. Bauer, C. Buscher, H. Wilmer, O. Hinrichsen, R. Becker, S. Rabe, K. Merz, M. Driess, R. A. Fisher and M. Muhler, *Catal. Lett.*, 2004, **92**, 49.
- (40) S. Posada-Pérez, J. R. d. S. Politi, F. Viñes and F. Illas, *RSC Adv.*, 2015, **5**, 33737.
- (41) P. Liu and J. A. Rodriguez, *J. Phys. Chem. B*, 2006, **110**, 19418.
- (42) J. Krzypek, M. Lachowska, M. Grzesik, J. Sloczynski and P. Nowak, *Chem. Eng. J.*, 1995, **58**, 101.
- (43) S.S. Iyer, T. Renganathan, S. Pushpavanam, M.V. Kumar and N. Kaisare, *J. of CO₂ Util.* 2015, **10**, 95.
- (44) L. C. Grabow and M. Mavrikakis, *ACS Catal.*, 2011, **1**, 365.
- (45) C. Liu, B. Yang, E. Tyo, S. Seifert, J. DeBartolo, B. von Issendorff, P. Zapol, S. Vajda and L. A. Curtiss, *J. Am. Chem. Soc.*, 2015, **137**, 8676.

-
- (46) F. Studt, M. Behrens, E. L. Kunkes, N. Thomas, S. Zander, A. Tarasov, J. Schumann, E. Frei, J. B. Varley, F. Abil-Pedersen, J. K. Norskov and R. Schlogl, *Chem. Cat. Chem.*, 2015, **7**, 1105.
- (47) T. Fujitani, Y. Choi, M. Sano, Y. Kushida, J. Nakamura, *J. Phys. Chem. C*, 2000, **104**, 1235.
- (48) M. Bowker, R. A. Hadden, H. Houghton, J. N. K. Hyland and K. C. Waugh, *J. Catal.*, 1987, **104**, 109.
- (49) J. R. B Gomes and J. A. N. F. Gomes, *Surf. Sci.*, 2000, **446**, 283.
- (50) J. R. B Gomes and J. A. N. F. Gomes, *Electrochim. Acta*, 1999, **45**, 653.
- (51) P. A. Taylor, P. B. Rasmussen, and I. Chorkendorff, *J. Chem. Soc. Faraday Trans.*, 1995, **91**, 1267.
- (52) J. Nerlov and I. Chorkendorff, *Catal. Lett.*, 1998, **54**, 171.
- (53) P. B. Rasmussen, P. M. Holmblad, T. Askgaard, C. V. Ovesen, P. Stoltze, P. J. K. Nørskov and I. Chorkendorff, *Catal. Lett.*, 1994, **26**, 373.